Physica Medica 66 (2019) 1–7

Contents lists available at ScienceDirect

Physica Medica

journal homepage: www.elsevier.com/locate/ejmp

Original paper

Dose perturbation and inhomogeneity of multi-arrays of ^{125}I seed-loaded stent for treatment of portal vein tumor thrombosis

Seongmoon Jung[a], Sui Shen[b], Sung-Joon Ye[a,c,*]

[a] Biomedical Radiation Sciences, Department of Transdisciplinary Studies, Graduate School of Convergence Science and Technology, Seoul National University, Seoul, South Korea

[b] Department of Radiation Oncology, University of Alabama at Birmingham Medical Center, Birmingham, AL, USA

[c] Robotics Research Laboratory for Extreme Environment, Advanced Institutes of Convergence Technology, Seoul National University, Suwon, Gyeonggi-do, South Korea

ARTICLE INFO

Keywords:
Portal vein tumor thrombosis
^{125}I seed-loaded stent
Monte Carlo
Dose perturbation

ABSTRACT

Purpose: To investigate the dosimetry of ^{125}I seed-loaded stent system currently used for an adjuvant treatment of portal vein tumor thrombosis (PVTT).

Methods: The stent system consisted of an inner metallic stent and outer seed–loaded capsules. Four arrays of ^{125}I seeds were attached longitudinally to the outer surface of the stent at 90° separation. 145 Gy was prescribed at 5 mm from the axes of seed-arrays. For the geometries of the 4-array, and potential 6- and 8-array configurations, treatment planning system (TPS) and Monte Carlo (MC) calculations were performed to evaluate 3D dose distributions and dosimetric impact of the metallic stent.

Results: The MC simulations indicated the metallic stent reduced a dose to the prescription points by over 10%, compared to the water-based TPS results. The total activity calculated by the water-based TPS to deliver the prescription dose should compensate for this amount of reduction. The MC- and TPS-calculated doses normalized to the prescription points for the current configuration were in agreements within 4.3% on a cylindrical surface along 5 mm from the axes of seed-arrays. The longitudinal underdosage worsened as approaching the edge of arrays, and ranged from 2.8% to 25.5%. The angular underdosage between neighboring arrays was 2.1%–8.9%.

Conclusions: With this compensation and a special care of near-edge underdosage, the current 4-array system can provide adequate dose coverage for treatment of PVTT. Further dosimetric homogeneity can be achieved using 6-or 8-array configurations.

1. Introduction

Portal vein tumor thrombosis (PVTT) is a common phenomenon in advanced stage hepatocellular carcinoma (HCC), with a prevalence rate ranging from 10% to 60% [1]. Patients with HCC and PVTT have a dismal prognosis, with an expected survival of 2–4 months with the best supportive care [2]. Systemic therapy with Sorafenib is the current standard treatment, recommended by the Barcelona Clinic Liver Cancer (BCLC) staging system [3,4], although, survival benefit following Sorafenib administration is modest, with a median survival time of 5.6–8.1 months [5,6]. Recently, intraluminal brachytherapy using ^{125}I seeds has emerged as an adjuvant treatment to provide local regional control of PVTT, and the results have revealed improved portal patency and overall survival [7–10]. Improved from loose-seeds-implant, array-seeds-stent system was developed. Improved outcomes in stent patency and survival in malignant esophageal and biliary obstruction have been demonstrated [11–13], as well as feasibility and safety in the treatment of PVTT caused by HCC [14].

The array-seeds stent exhibits promise for combining recanalization of an occluded portal vein and brachytherapy for tumor suppression. Previous dosimetry studies on array-seeds stent assessed the variation of dose distributions for various lengths of array-seeds stent and the number of seeds in each array, while ignoring the presence of metallic stent used for malignant biliary obstruction and PVTT patients [15,16]. Recently, the dose heterogeneity due to the metallic stent and guidewires in the intravascular brachytherapy were investigated [17,18]. However, dosimetric properties of the current clinical practice implemented 4-array-seeds stent for PVTT have not been fully evaluated. Because deficiency of dose uniformity (cold spot) might lead to inferior clinical outcome, the current study assessed the dosimetric effects due to the metallic stent, the angular uniformity of the dose distribution at various longitudinal cross-sections, using Monte Carlo (MC) techniques

* Corresponding author at: Seoul National University Hospital, 101 Daehangro, Jongno-Gu, Seoul 03080, South Korea.
E-mail address: sye@snu.ac.kr (S.-J. Ye).

https://doi.org/10.1016/j.ejmp.2019.09.077
Received 17 May 2019; Received in revised form 26 July 2019; Accepted 11 September 2019
Available online 26 September 2019

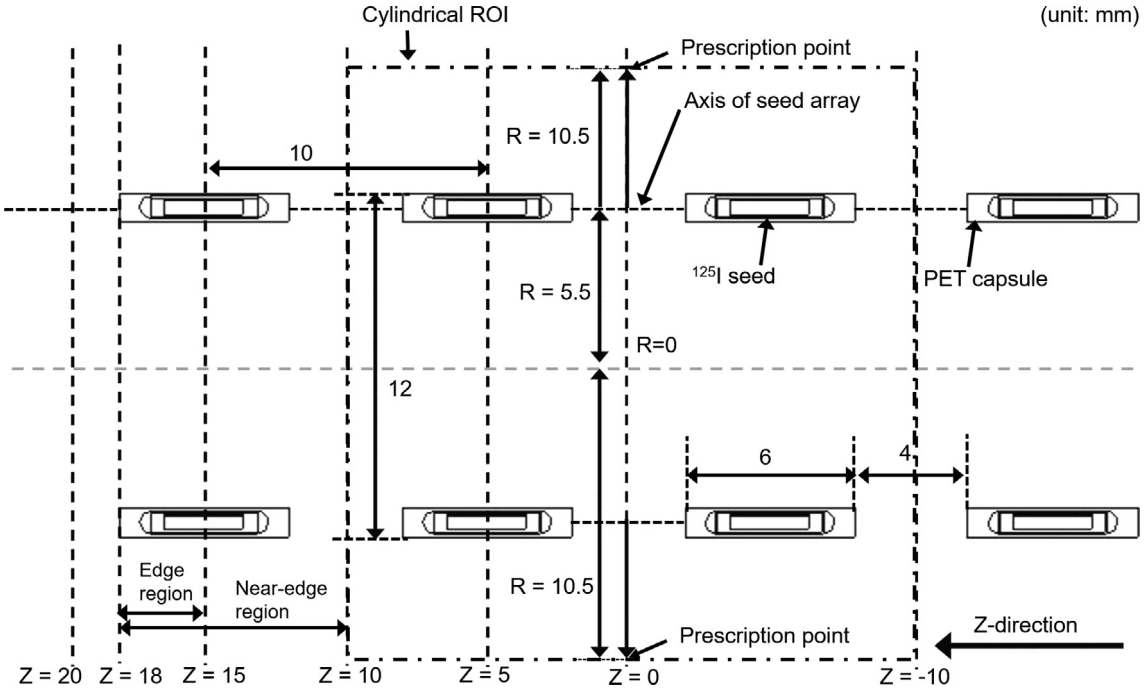

Fig. 1. Coordinate system in unit of mm on longitudinal plane of multi-arrays of ^{125}I seed-loaded stent at θ = 0°. *R* is the radial distance from the central axis of stent and *Z* is the longitudinal distance from the center of stent.

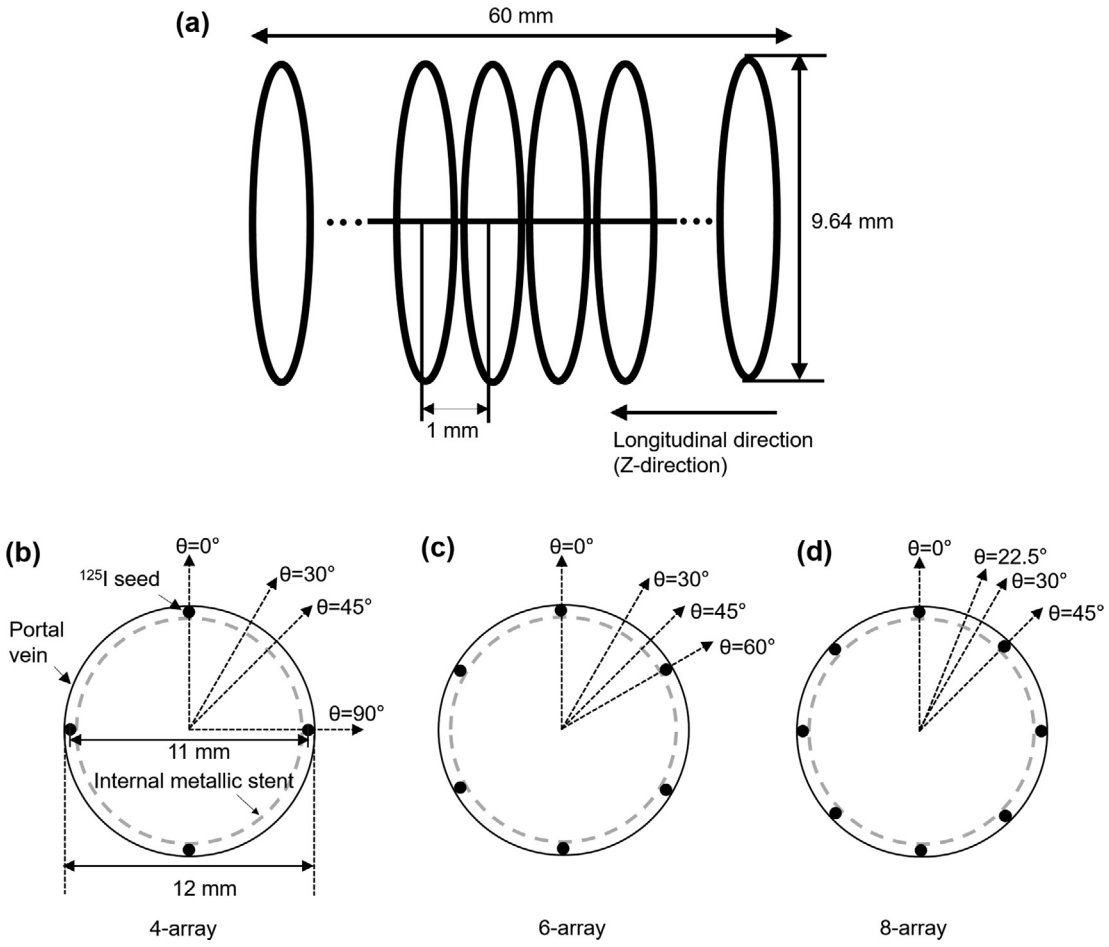

Fig. 2. (a) Ring geometry of metallic stent stent and schematic illustration on transverse plane of (b) 4-array, (c) 6-array and (d) 8-array of ^{125}I seed-loaded stent at Z = 5 mm.

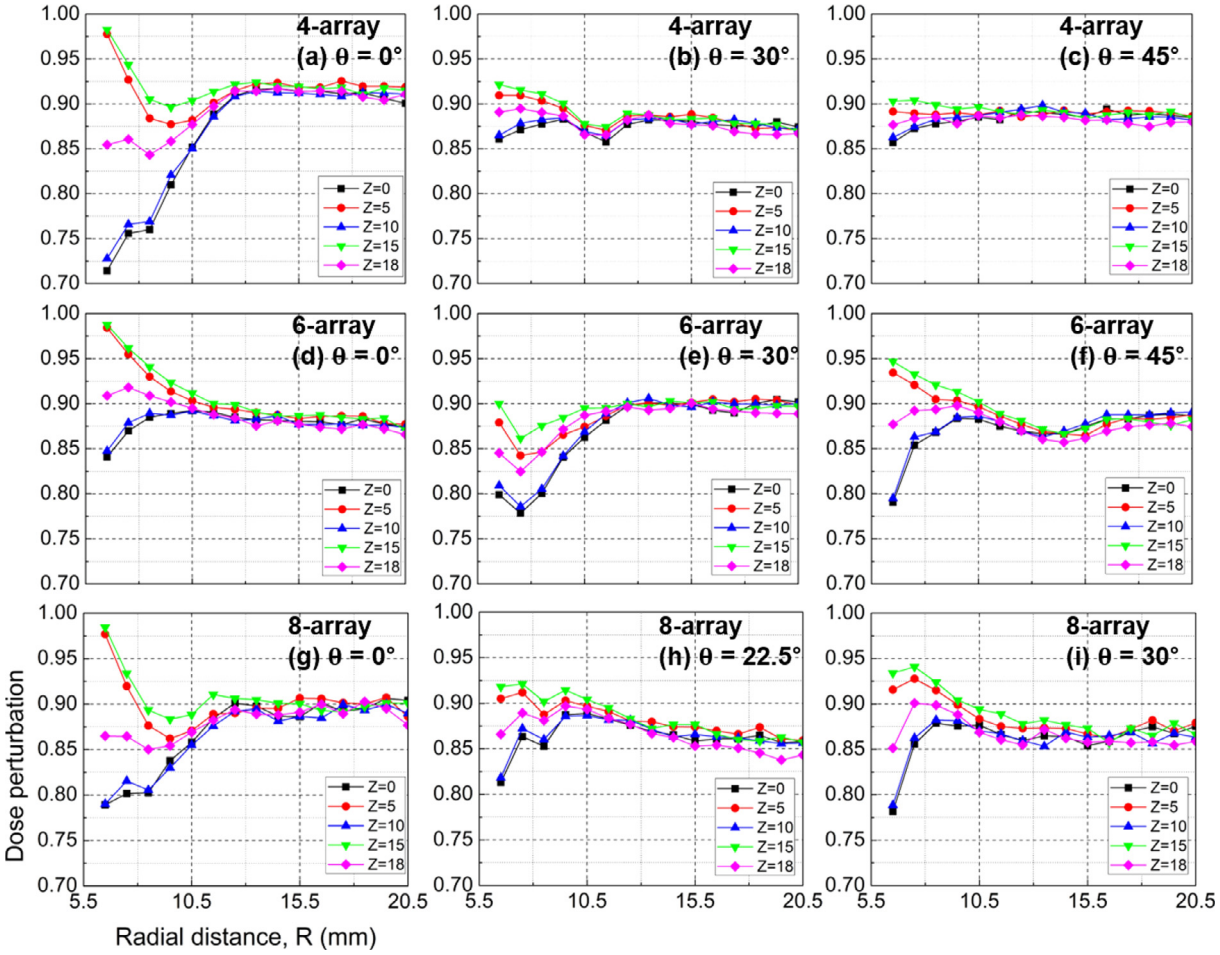

Fig. 3. Dose perturbation factors for (a-c) 4-arrays, (d-f) 6-array and (g-i) 8-array of ^{125}I seed-loaded stent.

and a commercial treatment planning system (TPS).

2. Material and methods

2.1. Array-seeds stent system

The portal vein array-seeds stent system has two separate parts that are coaxially deployed, consisting of an outer stent with polyethylene glycol terephthalate (PET) seed capsules (Nanjing MicroInvasive Medical Inc, Nanjing, China) and an inner self-expandable nitinol commercial stent (Luminexx III [Bard Peripheral Vascular, Inc, Tempe, Arizona] or S.M.A.R.T. Control [Cordis Corp, Miami Lakes, Florida]). The apparent radioactivity of each ^{125}I seed (CIAE-6711; Chinese Atomic Energy Science Institution, Beijing, China) ranged from 14.8 to 33.3 MBq. The principal photon emissions are 27.202, 27.472, 30.98, 31.71 keV for x-rays and 35.492 keV for γ-ray [19]. The length of the stent depends on the length of the obstructed segment. Various sizes of ^{125}I array-seeds stent are available at a diameter of 12–14 mm and a length of 60–100 mm. The size at a diameter of 12 mm and a length of 60 mm is most frequently used. The current array-seeds stent system consists of 4-array of seeds uniformly attached to the outer surface of the stent at 90° separation. The separation between the seeds is 4 mm in the longitudinal direction.

Stent placement is performed under fluoroscopic and ultrasound guidance. After puncturing, the patent second-order portal branch is punctured and reached using the Neff Percutaneous Access Set (Cook, Inc., Bloomington, Indiana). A guidewire (Boston Scientific, Marlborough, Massachusetts) is exchanged into the superior mesenteric vein through a 10-F sheath (Terumo, Tokyo, Japan). The outer stent is first implanted and the inner stent is immediately followed.

2.2. Prescription

In ^{125}I seed implants for liver metastasis, a minimal peripheral dose of 144 Gy to the target volume was used to determine radioactivity and the number of ^{125}I seeds to be implanted [20–22]. A similar dose prescription has been employed in our treatment of HCC with PVTT using array-seeds stent system. Prescription points were located at 5 mm from the axis of each array on the mid-transverse plane of the stent (Fig. 1). The prescription dose was 145 Gy at these points. A cylindrical region of interest (ROI) was defined in the longitudinal direction between Z = ± 10 mm, with its circular surface across four prescription points and an inner radius of 10.5 mm (see also Fig. 1). The edge region was defined as part of ROI between the center of the end seeds and 3.0 mm outward from it (Fig. 1). The near-edge region was defined as part of ROI between Z = ± 10 and Z = ± 18 mm.

2.3. Monte Carlo simulation

Monte Carlo N-Particle transport code version 6.1 (MCNP 6.1) was used to perform dose calculations [23]. The geometry of ^{125}I seed model 6711 was derived from that of Dolan *et al* [24]. The diameter of the array-seeds stent system and the inner diameter of portal vein were assumed to be 12 mm, the size widely used in the clinics. All space except the seeds, the metallic stent and PET capsules was assumed to be water. The cylindrical water phantom having a diameter of 12 cm and a length of 14 cm should be large enough to take into account backscattering [19,25]. As reported by Dolan *et al.* [24], the 6711 source

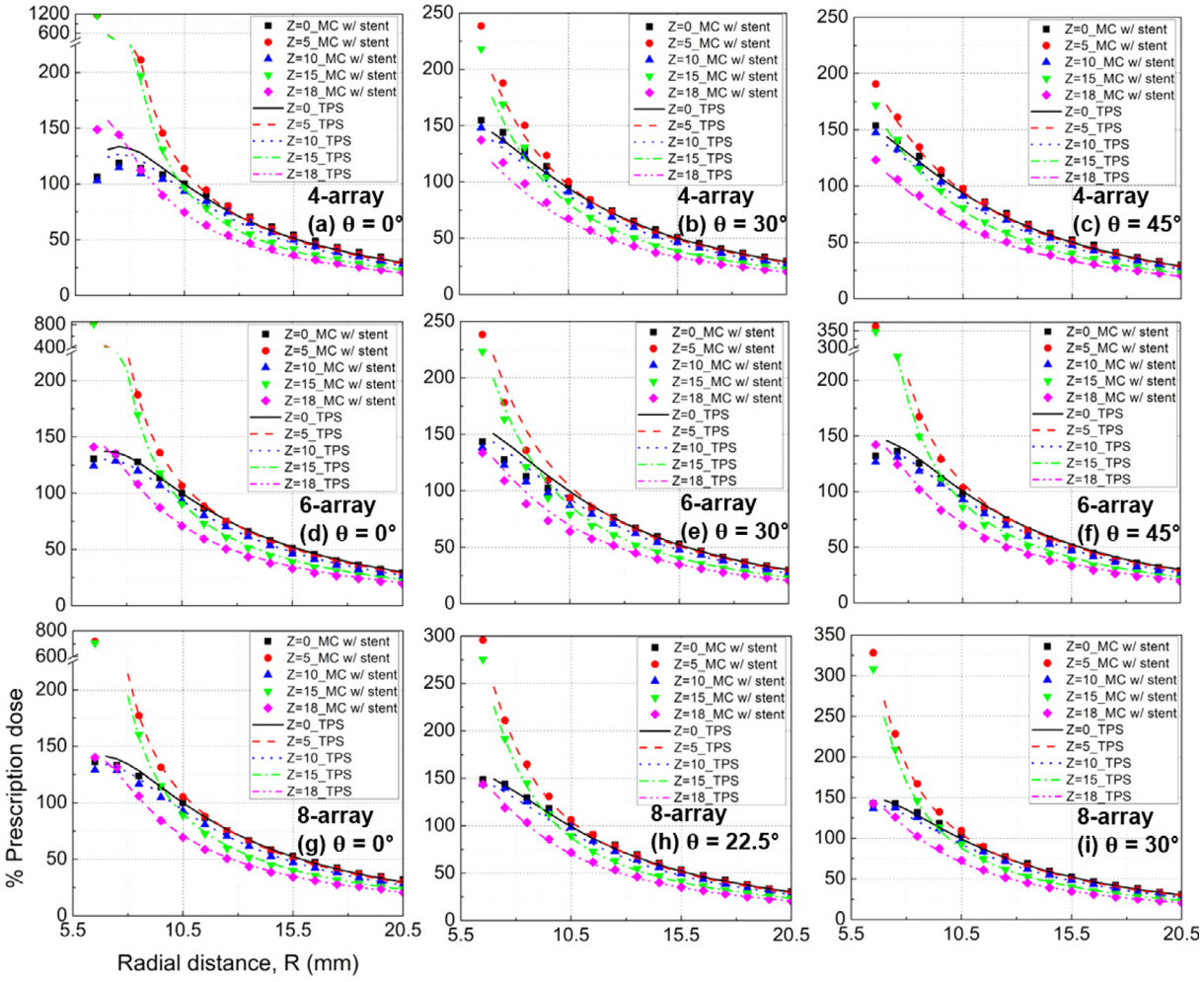

Fig. 4. MC-and TPS-calculated radial dose distributions for (a-c) 4-array, (d-f) 6-array and (g-i) 8-array of ^{125}I seed-loaded stent.

was encased inside a cylindrically symmetric titanium shell and had a cylinder of sliver coated with a radioactive layer. The radioactive layer consists of a mixture of AgBr and AgI. The dosimetric impact of internal metallic stent was evaluated by detailed MC simulations including a nickel alloy stent. It was difficult to implement a complex mesh geometry of the stent (e.g., Luminexx III or S.M.A.R.T. Control in this study) in MC simulations. A ring geometry of stent that has the same metallic surface area as the mesh stent was used for MC simulation as shown in Fig. 2(a) [26]. The outer diameter and the thickness of the ring stent were 9.64 mm and 0.16 mm respectively. Total sixty rings with a 1.0 mm gap between adjacent rings covered 60 mm length of the lesion site. The nickel alloy wires of which diameter and length were 0.18 mm and 52 mm, respectively, were included between the metallic stent and the seeds. These wires hold the seeds longitudinally. The metallic stent and the wire were made of 56% nickel and 44% titanium by weight. Taking into account the geometry from Fig. 2(b, c and d), 16, 24 and 32 ^{125}I seeds located at $R = 5.5$ mm were defined to be the sources for three different configurations. R is the radial distance from the central axis of the stent and θ is the angle defined in Figs. 1 and 2. Z is the longitudinal distance from the center of stent. Following the recommended nuclear data for ^{125}I [19], the five principle photons were emitted. A cylindrical mesh tally (cmesh type 3 in MCNP 6.1) was used with 1 mm (ΔR) × 1 mm (ΔZ) ×1° ($\Delta\theta$). R and Z ranged from 6.5 mm to 26.5 mm and −28.0 mm to 28.0 mm, respectively, while θ ranged from 0° to 360°. Hence, the voxel size ranged from 0.11 mm^3 to 0.46 mm^3. The statistical uncertainty (as Type A evaluation) in deposited energy was below 1% in all voxels. A cutoff energy for the photon transport was 1 keV. All MC simulated dose values were normalized to the dose value at the prescription points.

The dose perturbation due to the metallic stent was determined as a ratio of the doses with and without the metallic stent. Radial dose distributions at $\theta = 0°, 30°, 45°$ for 4-array, 6-array and $\theta = 0°, 22.5°, 30°$ for 8-array were also compared along the Z direction. In order to assess the dose coverage of each configuration, the ratio of two areas in a 100% isodose curve and a circle of $R = 10.5$ mm except the portal vein were calculated.

An initial air-kerma strength per ^{125}I seed to deliver the prescription dose to the prescription point, S_k, was compared for each configuration. First, an air-kerma strength conversion factor (Γ_k, (*unit of* $cGy{\cdot}cm^2{\cdot}mCi^{-1}{\cdot}h^{-1}$) was calculated by *in vacuo* MC modeling of a ^{125}I seed and a detector in air. The detector located at 10 cm apart from the seed was an air voxel of 2.7×2.7×0.05 cm^3 that was considered to be a wide-angle free air chamber [27]. An energy deposition tally (i.e., F6 tally in MCNP 6.1) was used to calculate the air-kerma in the detector. Assuming that an activity of ^{125}I seed was 3.7×10^7 Bq (i.e., 1 mCi), Γ_k was determined. An initial activity, A_0 needed to deliver 145 Gy to the prescription points was calculated by Eqs. (1) and (2):

$$d_p\left[\frac{Gy}{decay}\right] = 1.4757\left[\frac{photons}{decay}\right] \times \text{Dose per history}\left[\frac{Gy}{photon}\right] \quad (1)$$

$$D_p[Gy] = \int_0^\infty A_0 \cdot d_p \cdot e^{-\lambda t} dt = \int_0^\infty \dot{D}_0 \cdot e^{-\lambda t} dt \quad (2)$$

where d_p and D_p are a dose per decay and the cumulative prescription

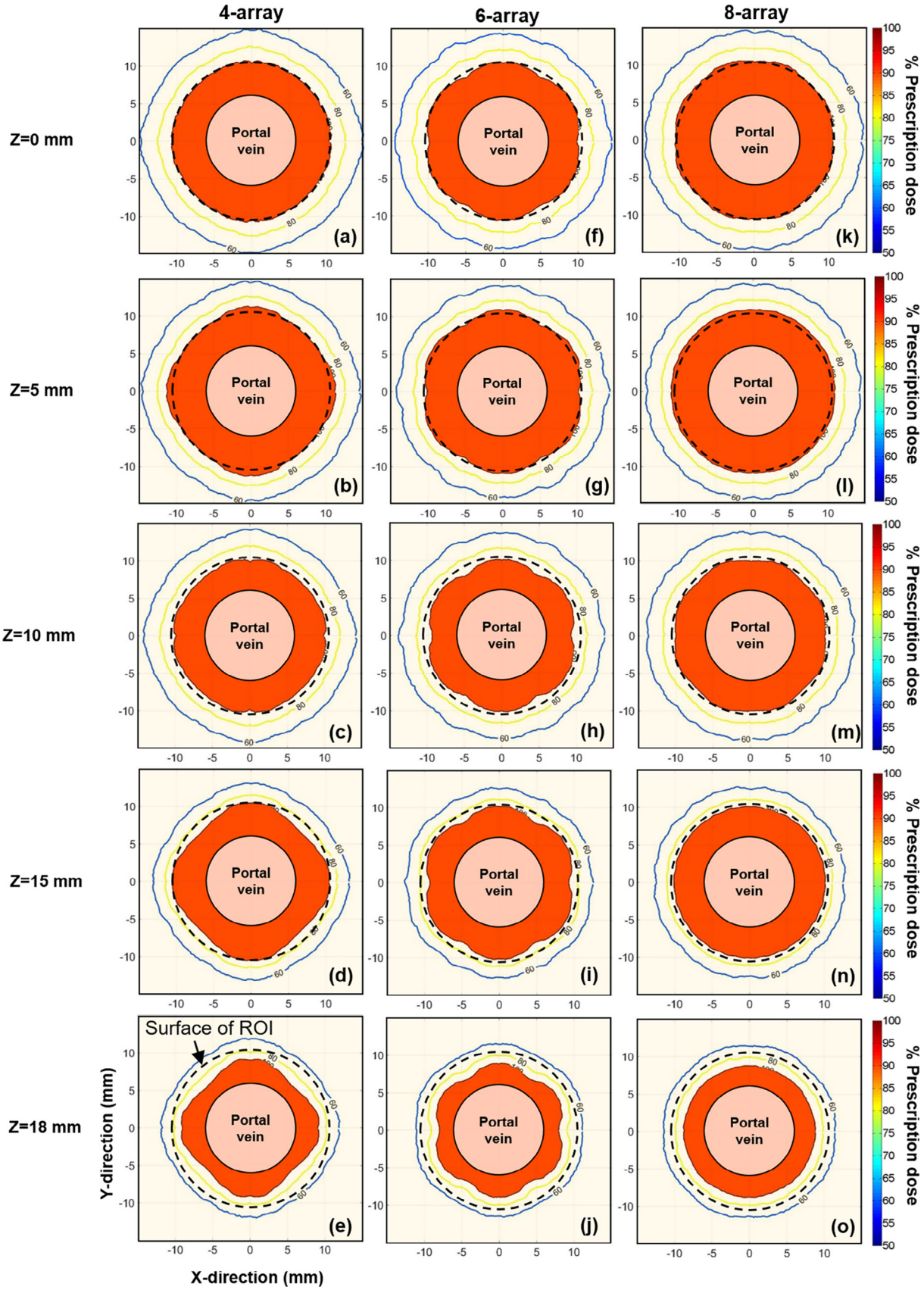

Fig. 5. MC-calculated 2D dose distributions on four transverse planes in column for three different configurations of ^{125}I seed-loaded stent in row. Red areas are within 100% isodose curves. (For interpretation of the references to colour in this figure legend, the reader is referred to the web version of this article.)

Table 1
Ratio of the areas inside a 100% isodose curve and a circle of radius = 10.5 mm (distance from the center of portal vein to the prescription point) except portal vein.

Longitudinal position Z (mm)	Seed-loaded stent configuration		
	4-array	6-array	8-array
0	1.00	0.94	1.03
5	1.08	1.04	1.12
10	0.87	0.82	0.91
15	0.84	0.82	0.88
18	0.52	0.50	0.54

Table 2
Initial air-kerma strength calculated by MC and TPS to deliver 145 Gy to the prescription point.

Seed-loaded stent configuration	4-array		6-array		8-array	
	MC w/ stent	TPS	MC w/ stent	TPS	MC w/ stent	TPS
Air-kerma strength per ^{125}I seed (cGy•cm^2/h)	1.038	0.901	0.683	0.619	0.547	0.473

dose (i.e., 145 Gy) at the prescription points, respectively. 1.4757 is the number of emitted photons per one decay [19] and a dose per history was calculated by MCNP 6.1. λ is a decay constant and t was a decay time. The values of S_k for each configuration were then calculated by Eq. (3).

$$S_k = \Gamma_k \times A_0 \quad (3)$$

2.4. Treatment planning system calculation

The same calculations were also performed with a clinical brachytherapy TPS (BrachyVision: Varian Medical Systems Inc., Palo Alto, CA). The ^{125}I seed model of 6711 was incorporated into the planning system, where the active length of the seed was 3 mm with an active diameter of 0.5 mm. Because the smallest radial distance listed in the standard TG-43 2D anisotropy function table was 5 mm [19], recent 2D anisotropic data for 6711 model were used in the current study [27]. While this 2D anisotropic data were in agreement with the consensus values of TG-43 [19], their radial distance started from 2.5 mm.

Three dimensional coordinates for individual seeds in the seed-loaded stent were manually entered into the treatment planning system with a spatial resolution of 0.1 mm. For each angular dose line profile on a particular plane, the starting point and ending point for each angular dose profile were calculated. Subsequently, the dose profile line was generated using these starting and ending points in the TPS. The numerical values of angular dose profile were exported. While the 3D dose grid was computed on 3D Cartesian coordinates, and angular dose line profile was on polar coordinates, the positional uncertainties associated with this method was < 0.05 mm. In water-based TG-43 dose calculations, dose perturbations due to outer sheathes (PET capsules), metallic stent and other metallic seeds nearby were totally ignored.

3. Results

3.1. Dose perturbation due to metallic stent

Dose perturbations on radial doses of 4-array, 6-array, and 8-array system at Z = 0, 5, 10, 15, and 18 mm are shown in Fig. 3. The dose reduction was observed for all three array systems. Particularly, the doses at the prescription points were decreased by 10.8%-14.8% when the stent was present. The radial dose perturbations before the prescription points (i.e., R = 10.5 mm, Z = 0 and θ = 0°) had relatively large fluctuations of 72% to 98%, nevertheless, the radial dose perturbations ranged from 88% to 92% beyond the prescription points.

3.2. Radial dose distribution

Radial dose distributions of 4-array system at Z = 0, 5, 10, 15, and 18 mm are shown in Fig. 4(a)-(c) for θ = 0°, 30°, and 45°. In these figures, the radial doses from MC with the stent and TPS agreed within 4.3% on the surface of ROI (i.e., cylindrical surface of R = 10.5 mm and Z = 0 to ± 10 mm). The doses near the surface of the ^{125}I seeds (i.e., R = 6.5 to 7.0 mm, θ = 0° and Z = 5 or 15 mm) were about several times higher than the prescription dose. The doses at the edge were only 66.2% to 74.5% of prescription dose for all three angles. The doses on the surface of ROI were over 91.1% of prescription dose for all three angles.

Radial dose distributions of 6- and 8-array systems at Z = 0, 5, 10, 15, and 18 mm are shown in Fig. 4(d)-(i) for different angles. The MC- and TPS-calculated doses on the surface of ROI agreed within 10.7% and 5.6% for 6- and 8-array systems, respectively. The doses near the surface of the ^{125}I seeds (i.e., θ = 0°, R = 6.5 mm and Z = 5 or 15 mm) were about 8.4 times higher for 6-array and 7.2 times higher than the prescription doses for 8-array. All the doses on the surface of ROI were over than 87.0% and 92.9% of prescription dose for 6- and 8-array systems, respectively. For 6-array, the MC doses in the edge region were 64.0% for θ = 30°and 69.3% for θ = 45°, while the TPS doses in the same location were 69.5% for θ = 30°and 71.7% for θ = 45°. For 8-array, the MC doses in the edge region were 71.8% for θ = 22.5°and 72.8% for θ = 30°, while the TPS doses at the same location were 70.1% for θ = 22.5°and 70.2% for θ = 30°.

Fig. 5 illustrates MC-calculated isodose curves in transverse planes. A dashed circle at R = 10.5 mm represents an ideal 100% isodose curve. The red areas were the region inside the 100% isodose curve. For all three array-configurations, the red areas at Z = 0 and 5 mm covered the area of dashed circle adequately. However, for 4-array and 6-array at Z > 10 mm, cold areas were obvious inside the ideal 100% isodose curve. While the cold spots of 6-array at Z > 10 mm were noticeable at angles between the arrays (e.g., Fig. 5(i)), the 8-array system showed fair angular uniformity (Fig. 5(n)). Table 1 lists the ratio of the red area to the area of dashed circle except the portal vein. The ratios of area for 8-array at Z = 0 mm, Z = 5 mm and Z = 10 mm were higher than 0.91.

3.3. Air-kerma strength per seed (S_k)

With each seed of 0.64 cGy•cm^2/h from the manufacturer, the total cumulative doses for 4-, 6- and 8-array systems were 103, 150 and 196 Gy, respectively. The air-kerma strength per seed, S_k, required to deliver 145 Gy to the prescription point was determined subsequently. MC-and TPS-calculated S_k per ^{125}I seed for the three different array configurations was summarized in Table 2. MC-calculated Γ_k was 0.718 cGy•cm^2•mCi^{-1}•h^{-1}. As increasing the number of arrays, the air-kerma strength per seed appeared proportionally decreased. Due to the dose reduction by the metallic stent, the air-kerma strengths from MC simulations were 9.4%-13.5% higher than those from TPS calculations.

4. Discussion

An 8-array system could have improved angular dose uniformity and coverage. The 4-array system could deliver > 91.1% prescription dose within ROI, while the 6- and 8-array systems over 87.0% and 92.9%, respectively. However, the underdosage on the surface of ROI was estimated 2.1% − 8.9% in angles between seed-arrays. The 6-array system delivered a lower dose inside the ROI than the 4-array system. Using the 6-array system, the underdosage on the surface of ROI was up to 13% at θ = 30° between seed-arrays at Z = 10 mm. This underdosage could be reduced into 1.9% − 2.7% using the 8-array system. Large

drops of dose were observed near Z = 15 mm, especially at θ = 30° and 45° (i.e., 83.3% and 80.6% of prescription dose, respectively). This indicated that extra seeding outside a full length of PVTT is necessary to achieve an adequate coverage of prescription dose.

The dose distributions calculated from MCNP 6.1 and TPS had a few noticeable discrepancies, mainly near the surface of the seed and at the edges of the array. The TPS used in this study was based on tabulated TG-43 parameters derived in a water phantom using EGSnrc [27]. Therefore, the TPS does not account for scattering and attenuation between the seeds, although the geometric details of the seed-array were configured. In contrast, in MCNP 6.1, these inter-seed interactions and interactions with the metallic components were all taken into account. While a recent paper suggested that the metallic stent inside the seed-loaded stent system would not significantly affect the dose distributions [15], our MC results in the current study demonstrated dose perturbations due to the metallic stent. This dose reduction at the prescription points should be considered when determining the air-kerma strength of the seeds for a treatment. Since low-energy photons from ^{125}I seeds are mostly interacted through the photoelectric absorption, the tissue heterogeneity may result in differences in dose distributions, comparing to the dose calculated in the water phantom [28]. Due to the difference in the elemental composition of liver and blood comparing with the water [29], the dose calculated in the water phantom might be slightly overestimated. Moreover, calcifications in the portal vein are present in some cases. As reported by Meigooni *et al.* [30], the calcifications with 1.7% calcium contents may lead to 5% differences in the dose. Further, *in vivo*- or *in phantom*-dosimetry can be investigated for a dose verification of ^{125}I seed-loaded stent system for treatment of PVTT by measurements of TLDs [31–33].

Clinical applications using the 4-array-seeds stent have shown promising outcomes in delaying tumor growth and prolonging stent patency, including esophageal cancer, malignant biliary obstruction, malignant portal vein thrombosis, and malignant airway obstruction [11–14,34,35]. An improved dose uniformity and target coverage at the near-edge may, result in better outcomes in theory.

5. Conclusions

In treatment of PVTT using multi-arrays of ^{125}I seed stent, the impact of metallic stent turned out to be significant and led to underdosage to the lesion (approximately 10% in this study). If TPS could not account for heterogeneities in dose calculations, the total activity calculated by the TPS to deliver a prescription dose should compensate for this impact (i.e., dose reduction by metallic stent). When the TPS- and MC-calculated doses were normalized to the prescription points, the agreement between the two was within 4.3% on a cylindrical surface along the prescription distance from the axes of seed-arrays. With this compensation and a special care of near-edge underdosage, the current 4-array system can provide adequate dose coverage. Dosimetric homogeneity can be improved using 6-or 8-array configurations.

Declaration of Competing Interest

The authors declare that they have no known competing financial interests or personal relationships that could have appeared to influence the work reported in this paper.

Acknowledgements

This work was supported by the National Research Foundation of Korea (NRF) grant funded by the Korean government (MSIP: Ministry of Science, ICT and Future Planning) (No. NRF-2013M2B2B1075776).

References

[1] Chan SL, Chong CC, Chan AW, et al. Management of hepatocellular carcinoma with portal vein tumor thrombosis: Review and update at 2016. World J Gastroentero 2016;22:7289–300.
[2] Han K, Kim JH, Ko GY, et al. Treatment of hepatocellular carcinoma with portal venous tumor thrombosis: A comprehensive review. World J Gastroentero 2016;22:407–16.
[3] E.A.S.L.-E.O.R.T.C.. Clinical practice guidelines: management of hepatocellular carcinoma. J Hepatol 2012;56:908–43.
[4] Bruix J, Sherman M. Management of hepatocellular carcinoma: an update. Hepatology 2011;53:1020–2.
[5] Bruix J, Raoul JL, Sherman M, et al. Efficacy and safety of sorafenib in patients with advanced hepatocellular carcinoma: subanalyses of a phase III trial. J Hepatol 2012;57:821–9.
[6] Cheng AL, Guan Z, Chen Z, et al. Efficacy and safety of sorafenib in patients with advanced hepatocellular carcinoma according to baseline status: subset analyses of the phase III Sorafenib Asia-Pacific trial. Eur J Cancer 2012;48:1452–65.
[7] Zhang L, Mu W, Hu CF, et al. Treatment of portal vein tumor thrombus using ^{125}I seed implantation brachytherapy. World J Gastroentero 2010;16:4876–9.
[8] Chuan-Xing L, Xu H, Bao-Shan H, et al. Efficacy of therapy for hepatocellular carcinoma with portal vein tumor thrombus: chemoembolization and stent combined with iodine-125 seed. Cancer Biol Ther 2011;12:865–71.
[9] Luo JJ, Yan Z, Liu Q, et al. Endovascular placement of iodine-125 seed strand and stent combined with chemoembolization for treatment of hepatocellular carcinoma with tumor thrombus in main portal vein. J Vasc Interv Radiol 2011;22:479–89.
[10] Luo JJ, Zhang ZH, Liu QX, et al. Endovascular brachytherapy combined with stent placement and TACE for treatment of HCC with main portal vein tumor thrombus. Hepatol Int 2016;10:185–95.
[11] Guo JH, Teng GJ, Zhu GY, et al. Self-expandable esophageal stent loaded with ^{125}I seeds: initial experience in patients with advanced esophageal cancer. Radiology 2008;247:574–81.
[12] Zhu HD, Guo JH, Zhu GY, et al. A novel biliary stent loaded with ^{125}I seeds in patients with malignant biliary obstruction: preliminary results versus a conventional biliary stent. J Hepatol 2012;56:1104–11.
[13] Zhu HD, Guo JH, Mao AW, et al. Conventional stents versus stents loaded with ^{125}I seeds for the treatment of unresectable oesophageal cancer: a multicentre, randomised phase 3 trial. Lancet Oncol 2014;15:612–9.
[14] Lu J, Guo JH, Zhu HD, et al. Safety and efficacy of irradiation stent placement for malignant portal vein thrombus combined with transarterial chemoembolization for hepatocellular carcinoma: a single-center experience. J Vasc Interv Radiol 2017;28:786–94.
[15] Yao LH, Wang JJ, Shang C, et al. In vitro dosimetric study of biliary stent loaded with radioactive ^{125}I seeds. Chin Med J 2017;130:1093–9.
[16] Yao LH, Su L, Liu L, et al. Stenting of the portal vein combined with different numbers of iodine-125 seed strands: dosimetric analyses. Chin Med J 2017;130:2183–9.
[17] DeCunha J, Janicki C, Enger SA. A retrospective anaylsis of catheter-based sources in intravascular brachytherapy. Brachytherapy 2017;16:586–96.
[18] DeCunha JM, Enger SA. A new delivery system to resolve dosimetric issues in intravascular brachytherapy. Brachytherapy 2018;17:634–43.
[19] Rivard MJ, Coursey BM, DeWerd LA, et al. Update of AAPM Task Group No. 43 Report: a revised AAPM protocol for brachytherapy dose calculations. Med Phys 2004;31:633–74.
[20] Armstrong JG, Anderson LL, Harrison LB. Treatment of liver metastases from colorectal cancer with radioactive implants. Cancer 1994;73:1800–4.
[21] Martinez-Monge R, Nag S, Nieroda CA, et al. Iodine-125 brachytherapy in the treatment of colorectal adenocarcinoma metastatic to the liver. Cancer 1999;85:1218–25.
[22] Williamson JF, Butler W, DeWerd LA, et al. Recommendations of the American association of physicists in medicne regarding the impact of implementing the 2004 task group 43 report on dose specification for ^{103}Pd and ^{125}I interstitial brachytherapy. Med Phys 2005;32:1424–39.
[23] Goorley T, James M, Booth T, et al. Initial Mcnp6 release overview. Nucl Technol 2012;180:298–315.
[24] Dolan J, Lia Z, Williamson JF. Monte Carlo and experimental dosimetry of an ^{125}I brachytherapy seed. Med Phys 2006;33:4675–84.
[25] Ye SJ, Brezovich IA, Shen S, et al. Dose errors due to inhomogeneities in balloon catheter brachytherapy for breast cancer. Int J Radiat Oncol Biol Phys 2004;60:672–7.
[26] Li XA, Chibani O, Greenwald B, et al. Radiotherapy dose perturbation of metallic esophageal stents. Int J Radiat Oncol Biol Phys 2002;54:1276–85.
[27] Taylor RE, Rogers DW. An EGSnrc Monte Carlo-calculated database of TG-43 parameters. Med Phys 2008;35:4228–41.
[28] Oliveira SM, Teixeira NJ, Fernandes L, et al. Dosimetric effect of tissue heterogeneity for ^{125}I prostate implants. Rep Pract Oncol Raditother 2014;19:392–8.
[29] International Commission on Radiological Protection. Basic anatomical and physiological data for use in radiological protection: reference values. ICRP Publication No. 89. Oxford: Pergamon, 2002.
[30] Meigooni AS, Awan SB, Tompson NS, et al. Updated Solid WaterTM to water conversion factors for ^{125}I and ^{103}Pd brachytherapy sources. Med Phys 2006;33:3988–92.
[31] Jaselske E, Adliene D, Rudzlanskas V, et al. In vivo dose verification method in catheter based high dose rate brachytherapy. Phys Medica 2017;44:1–10.
[32] Chiu-Tsao ST, Astrahan MA, Finger PT, et al. Dosimetry of ^{125}I and ^{103}Pd COMS eye plaques for intraocular tumors: report of Task Group 129 by the AAPM and ABS. Med Phys 2012;39:6161–84.
[33] Oliver SCN, Leu MY, DeMarco JJ, et al. Attenuation of I-125 radiation with vitreous substitutes in the treatment of uveal melanoma. AMA Arch Ophthalmol 2010;128:888–93.
[34] Zhu HD, Guo JH, Huang M, et al. Irradiation stents vs. conventional metal stents for unresectable malignant biliary obstruction: a multicentre trial. J Hepatol 2018;68:970–7.
[35] Wang Y, Lu J, Guo JH, et al. A novel tracheobronchial stent loaded with ^{125}i seeds in patients with malignant airway obstruction compared to a conventional stent: a prospective randomized controlled study. EBioMedicine 2018;33:269–75.